



Article

Simultaneous Ultra-Fast Imaging and Neutron Emission from a Compact Dense Plasma Focus Fusion Device

Nathan Majernik, Seth Pree, Yusuke Sakai, Brian Naranjo, Seth Putterman and James Rosenzweig *

Department of Physics and Astronomy, University of California Los Angeles, Los Angeles, CA 90095, USA; NMajernik@g.ucla.edu (N.M.); sethlpree@gmail.com (S.P.); yusuke@physics.ucla.edu (Y.S.); brian.naranjo@gmail.com (B.N.); puherman@ritva.physics.ucla.edu (S.P.)

* Correspondence: rosen@physics.ucla.edu; Tel.: +310-206-4541

Received: 12 February 2018; Accepted: 5 April 2018; Published: 11 April 2018



Abstract: Recently, there has been intense interest in small dense plasma focus (DPF) devices for use as pulsed neutron and X-ray sources. Although DPFs have been studied for decades and scaling laws for neutron yield versus system discharge current and energy have been established (Milanese, M. et al., *Eur. Phys. J. D* **2003**, *27*, 77–81), there are notable deviations at low energies due to contributions from both thermonuclear and beam-target interactions (Schmidt, A. et al., *Phys. Rev. Lett.* **2012**, *109*, 1–4). For low energy DPFs (100 s of Joules), other empirical scaling laws have been found (Bures, B.L. et al., *Phys. Plasmas* **2012**, *112702*, 1–9). Although theoretical mechanisms to explain this change have been proposed, the cause of this reduced efficiency is not well understood. A new apparatus with advanced diagnostic capabilities allows us to probe this regime, including variants in which a piston gas is employed. Several complementary diagnostics of the pinch dynamics and resulting X-ray neutron production are employed to understand the underlying mechanisms involved. This apparatus is unique in its employment of a 50 fs laser-based shadowgraphy system that possesses unprecedented spatio-temporal resolution.

Keywords: dense plasma focus; neutron source; plasma pinch; shadowgraph

1. Introduction

A dense plasma focus (DPF) is a compact device, often termed a pinch, which produces high-density, energetic plasmas, used for production of radiation ranging from hard X-rays to fusion neutrons. This is achieved with a coaxial set of electrodes in a relatively low-pressure environment, connected to a pulsed, high voltage power source (Figure 1). During the first phase of operation, a fast switch is closed, energizing the DPF and causing a plasma sheath to form between the anode and cathode, initially along the surface of the insulator. This plasma sheath layer carries current in the radial direction, while the currents on the surface inner electrode that feed this radial current travel in the axial direction. This axial current gives rise to an azimuthal magnetic field, and the resultant magnetic force pushes the sheath current axially away from the base of the cathode. The resultant electromagnetic pressure-induced travel of the discharge sheath along the electrode is termed “run down”, and as it moves, the sheath collects the gas in front of it in a snowplow-like mechanism [1]. As the sheath crests over the top of the electrodes, its longitudinal motion takes it beyond the tip of the anode, so current begins to flow axially near the center. This gives rise to magnetic forces which produce a radial collapse along the top of the anode. This leads to a z-pinch scenario, which completes the “run in” process that serves to push the gas that had been plowed forward during the earlier

run-down. This radial collapse thus produces a temporarily self-sustaining, very hot and dense plasma region called the pinch.

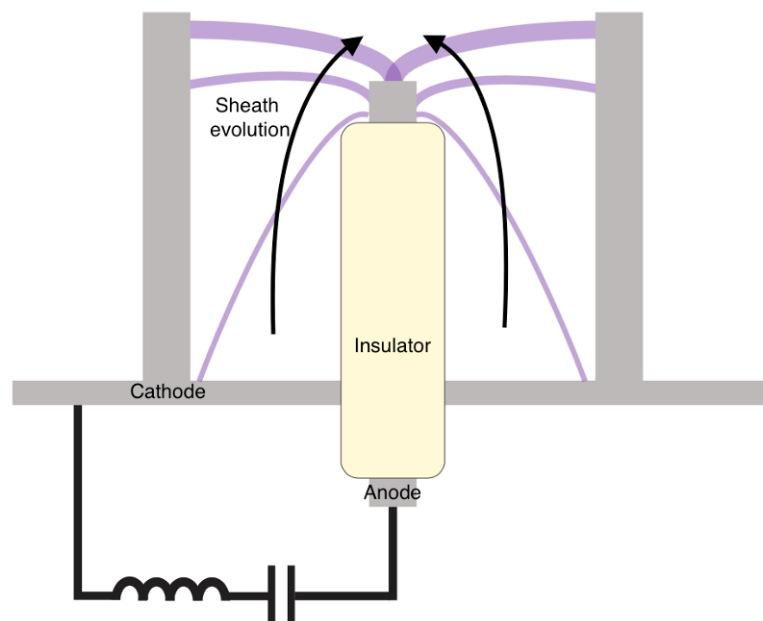


Figure 1. Schematic of a dense plasma focus device, or DPF.

The conditions inside of the DPF are that of a dense, collisional plasma with significant non-thermal velocity components. This scenario in turn produces copious radiation: electromagnetic radiation (to the hard X-ray spectrum) from the electrons; and, with appropriate gas, neutrons produced in fusion reactions between nuclei. The DPF pinch, though intense, is short-lived, so the radiation emitted by the creation of dense, energetic plasma is pulsed. As such, DPFs have been extensively studied for use as pulsed X-ray sources for applications including lithography and specialized radiography [2–4].

The interest of this current work, however, is in the use of DPFs as pulsed neutron generators. This is accomplished using gas blends which include deuterium and/or tritium. The configuration space density and velocity distributions within the pinch can indeed be sufficient to initiate D-D and D-T fusion events which liberate 2.45 MeV and 14.1 MeV neutrons respectively. Compared to radioactive sources, which are CW neutron sources or typical neutron generators with their millisecond to microsecond minimum pulse durations and rise times, DPFs offer an attractive way of producing relatively high fluxes of neutrons in very short (10–100 ns of nanoseconds) bursts. An industrial scale D-D neutron generator offers 10^{11} n/s [5]. This may be compared to a typical DPF generating 10^6 neutrons over a 10 ns pulse: 10^{14} n/s.

Since their first construction in the 1960s [6], DPFs have been built in a range of sizes and energies ranging from less than a joule [7] to a megajoule [8]. Within much of this range, neutron yield per shot generally scales with energy stored in the driver [9], incentivizing the construction of larger devices. Large devices come with their own host of problems however, including expense, size, low repetition rate, average power consumption, heat management, and electrode erosion. Additionally, at high discharge energies (>100 kJ), there are saturation effects that break the simple scaling law [10,11]. This has led to a recent proliferation of very small DPFs, often termed *nanofocus* devices [12–21]. The advantages of such small devices, in the 100 J range or below, found in their low cost, compactness, and flexible operating modes, are attractive, as is the short pulse length described above. These advantages are counterbalanced by the relatively low neutron yield per pulse, and techniques have been explored, such as the use of current transformers [22] and piston gases [23–28], to mitigate

the yield issue. The device we describe in this paper permits explorations of the physics of these smaller-scale DPFs.

2. Materials and Methods

The electrodes of our device are inspired by the work reported in [29] and consist of a copper anode, a borosilicate glass tube insulator, and 6 posts to form the cathode. The inner anode cylinder has an OD of 5.6 mm and an exposed length of 15 mm; the tip is aligned to the height of the cathode posts. To modify the run-in dynamics, a hole is bored in the center to a diameter of 2 mm and depth of 10 mm. The lower portion of the anode is surrounded by a borosilicate glass tube with OD of 9.5 mm. The posts which form the cathode are on a 17.5 mm diameter circle. Each of these stainless steel posts has a 4 mm diameter and extends 38 mm above the base of the cathode. The cathode base includes a 2 mm tall, 0.5 mm thick protrusion around the center hole which acts as a field enhancement element to improve the consistency of sheath formation. This configuration is shown in Figure 2. The driver circuit for this DPF consists of 212 nF of parallel ceramic capacitors, typically charged between 35 and 40 kV for a maximum stored energy of 170 J. The capacitor bank is switched by an atmospheric spark gap, with breakdown triggered by a 500 mJ Nd:YAG laser pulse. The layout of both the driver and transmission line has been designed to minimize the inductance which has been determined to be 70 nH. This yields a system with a peak current 70 kA and a 190 ns quarter period—the approximate time for run-down to take place.

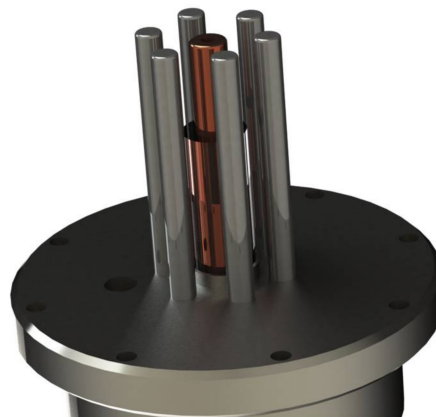


Figure 2. Rendered image of DPF electrodes with insulator around anode base, and a multi-post cathode configuration.

2.1. Diagnostics

A wide range of diagnostics is employed to understand the macroscopic and microscopic behavior of the system. The noisy RF environment produced by the powerful DPF discharges requires special considerations when selecting and designing instrumentation.

2.1.1. Electrical Diagnostics

One of the most essential type of electrical diagnostic employed is a custom B-dot probe to measure dI/dt , thus giving detailed insight into the macroscopic operational characteristics of the DPF. Most notably, a dip in this signal has been shown to correspond to a rapid change in impedance, indicating the creation of a successful pinch [18]. The information from these detectors is sometimes supplemented by an integrating current transformer and a high speed, high voltage probe.

3. Results

3.1. Example Shot

Figure 4 shows an example DPF shot, as visualized through multiple diagnostics. The blue trace is di/dt (measured by B-dot probe) and the current feature has been highlighted. The vertical blue lines indicate the time periods the framing camera images (below) are taken from. The green and red traces are the outputs from scintillator-PMT sensors at distances of 0.3 m and 1.6 m from the DPF respectively. The whole solid angle leading to these detectors was blocked by 7 mm of lead, which attenuates any X-rays below 100 keV to a negligible level while only slightly attenuating the fast neutrons. The gap between these two pulses, 60 ns, agrees with the time-of-flight expected from a 2.45 MeV neutron traversing 1.3 m of distance. Below that plot is a series of four images from the framing camera, showing the sheath strike, run down, and aftermath of the pinch.

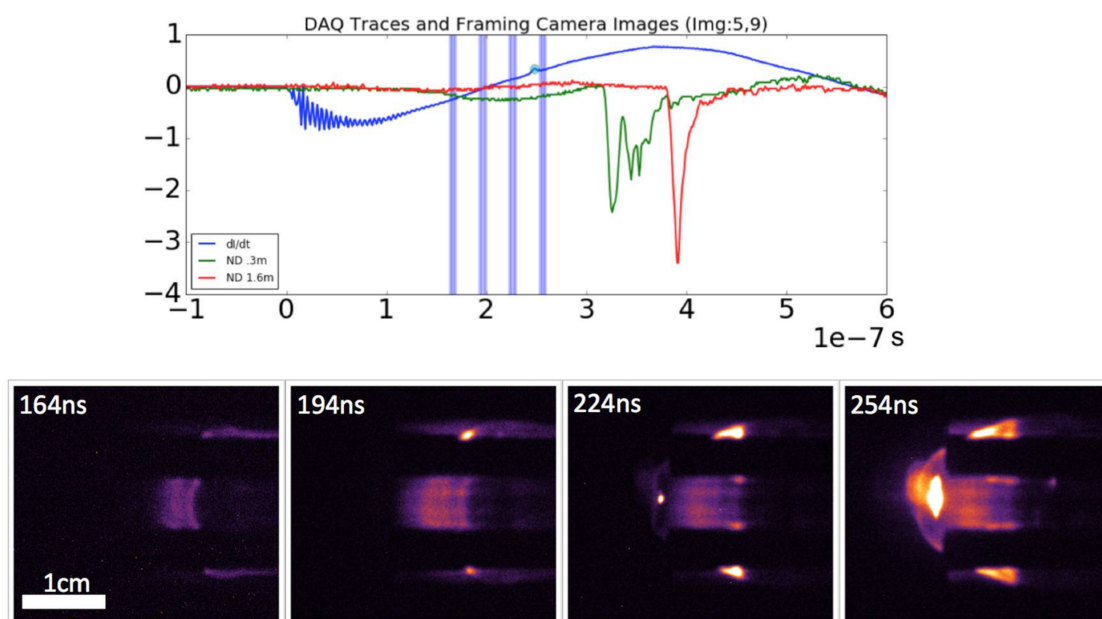


Figure 4. (Top) Current dip in di/dt signal from the B-dot probe (blue trace), along with the PMT time-of-flight measurements (red and green traces); synchronized with (bottom) a series of framing camera images separated by 30 ns.

3.2. Snowplow Model Validation

The snowplow model predicts the peak sheath velocity (through the “drive parameter”) [34] as a function of a , anode diameter, I_{max} , the peak current, and P , the ambient gas pressure, as:

$$v_z \propto \frac{I_{max}}{a \sqrt{P}} \tag{1}$$

The framing camera was used to take bursts images of DPF shots while pressure was swept. Using image analysis, the sheath progression after cresting the cathode was measured, the motion was interpolated, and the velocity was deduced. These values were calculated at several pressures and fit with a power curve, shown in Figure 5. The power to fit pressure to velocity was -0.55 , in good agreement with the snowplow model’s projection of -0.5 .

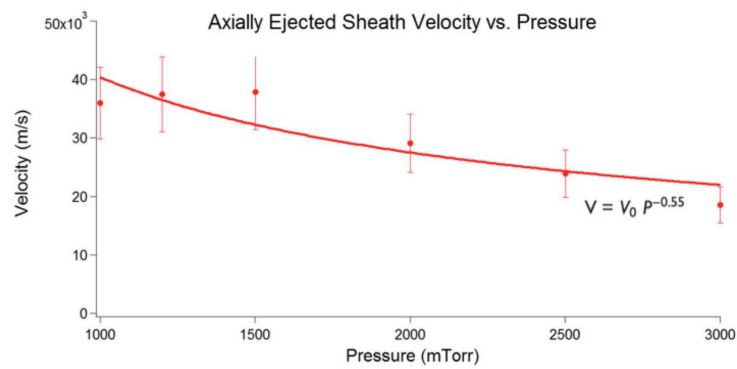


Figure 5. Measured peak sheath velocity as a function of pressure at fixed voltage.

3.3. Shadowgraph Imaging

Even with the fastest possible shutter speed for the framing camera (3 ns), the plasma sheath, moving at 50 km/s, would smear over 150 microns. The ultra-fast laser used for imaging allows capture of even the fastest plasma dynamics without any motion blur. In fact, the system's temporal resolution is not limited by the laser pulse duration (50 fs) but the speed of light transit across the anode (17 ps). Due to the use of an atmospheric spark gap though, there is significant (ns) jitter despite the synchronization between the imaging laser (Ti:Sapphire) and the trigger laser (Nd:YAG). For this reason, the phase of the image relative to the RLC oscillation must be determined ex post facto. Since the jitter is stochastic, many shots are taken to image the phases of interest with sufficient granularity.

An example of the multi-shot shadowgraph imaging is shown in Figure 6, demonstrating the radial run-in of the plasma sheath across the anode face.

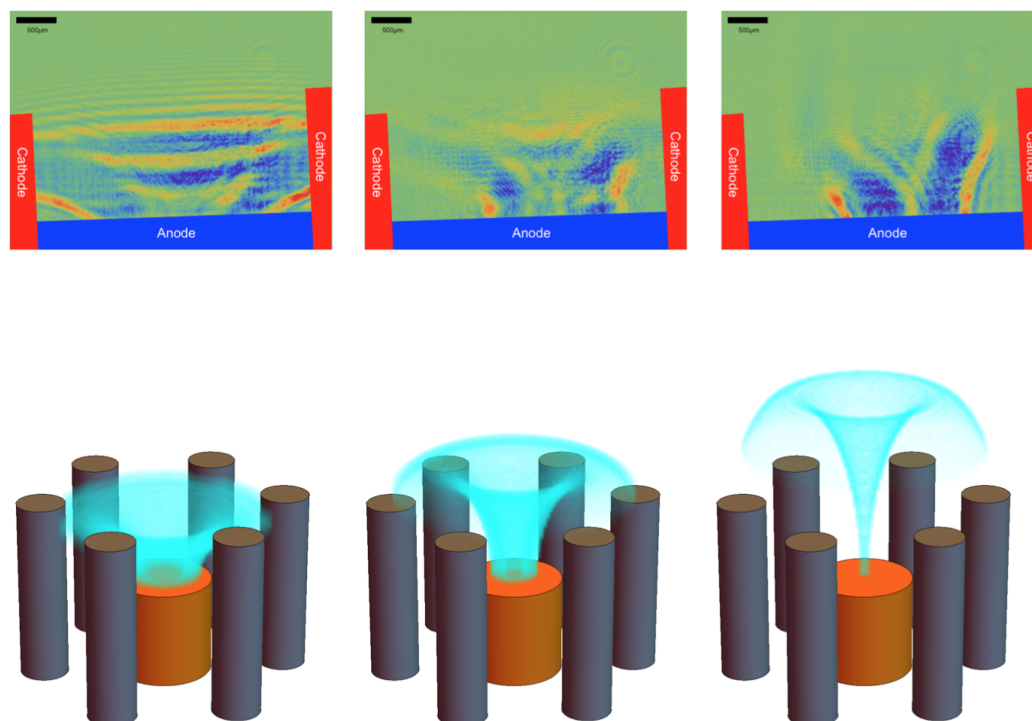


Figure 6. The **top** row shows shadowgraph images showing the progression of the plasma sheath run-in. The **bottom** row is a schematic representation of the run-in to clarify the shadowgraphy.

3.4. Neutron Yield

To determine the neutron yield of this compact DPF system, 4 scintillator/PMT units were placed 2.8 m from the PMT and shielded with 7 mm of lead. This increased distance was to reduce the likelihood of pileup on the detectors, which are intended for detecting single neutron events.

The highest yield results from a fill pressure of 6.45 Torr using this DPF geometry and circuit. The pressure was maintained by a PID controller with a vacuum pump consistently removing gas through an aperture. The gas was entirely purged and replaced every 100 shots.

A binomial distribution is assumed for each of the four detectors, each with their own efficiency $pDet_i$ which accounts for the intrinsic efficiency of the scintillator, PMT, distance from the DPF, and shielding. For a given yield, the probability of a particular detector, i , registering a hit is $p_i = 1 - (1 - pDet_i)^{yield}$ and the probability of not registering a hit is $q_i = 1 - p_i$. The four detectors signals are treated as independent events so, given the relevant $pDet_i$ values and the yield, one can calculate the probability of obtaining 0, 1, ..., 4 hits among the four detectors for each shot of the DPF. This is summarized in Figure 7. Using these relationships and measured data, we can calculate coefficients of a Poisson distribution for the neutron yield. We note that there is a precedent for using a Poisson distribution to describe neutron yield [35,36]. The best fit distribution is shown in Figure 8. To corroborate these results, the values of $pDet_i$ can be varied either by shielding or changing the distance to the detector (reducing the solid angle coverage). We opted to use paraffin slabs of thicknesses from 5 to 15 cm (backed by 1 cm of lead to stop secondaries) to attenuate the neutron signal in a controllable way. GEANT [37] simulations confirmed that a controllable fraction of the (effectively monochromatic) neutrons initially produced would be unmoderated by the paraffin. By using a time window exclusion and our tightly time resolved neutron detectors, we can still selectively measure full energy neutrons but with less chance of pileup.

This corresponds to a mean yield of 37,000 n /shot, a 10th percentile yield of 65,000 n /shot, and a 1st percentile yield of 125,000 n /shot.

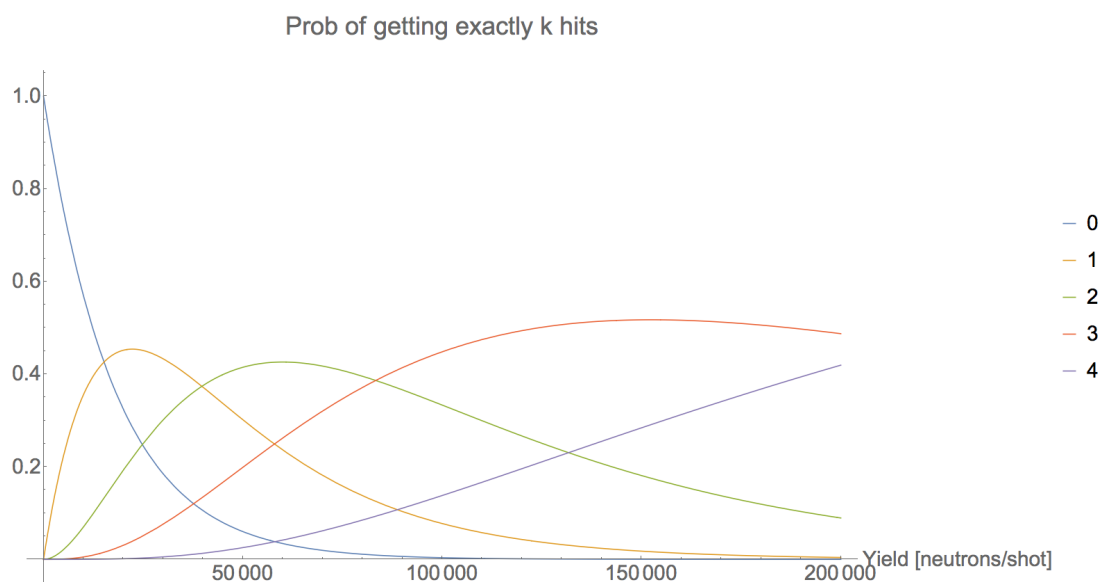


Figure 7. The probability of getting exactly k detected neutrons from a single shot, given the detection system parameters used and the shot yield.

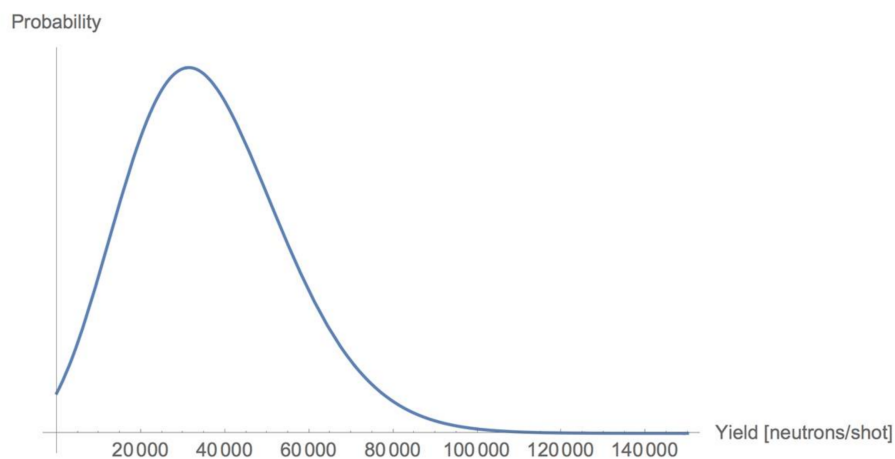


Figure 8. Best fit Poisson distribution for neutron yield in our optimized DPF.

Soto [38] established an empirical scaling law for neutron yield, which is particularly for small (<1 kJ) DPFs:

$$Y \approx 7.73 \cdot 10^{-5} I_0^{4.82}, \quad (2)$$

where Y is the expected yield per shot and I_0 is the peak current in kA. Based on this scaling law and our system parameters we expect to produce about 30,000 neutrons per shot. The overall predictions of the Soto model have been validated, or even exceeded in this device.

3.4.1. Double Strike

By virtue of the tight temporal resolution of the neutron detection system, a small fraction of DPF shots were found to contain two distinct neutron emission periods, typically separated by half of an RLC period. Such a phenomenon has been mentioned in passing by other researchers [39] but has not been explored. Despite attempts to tune system parameters to increase the frequency of these double strike events, they were never reliably and consistently produced.

3.4.2. Noble Gas Doping

Running DPFs with an admixture of deuterium and a heavy noble gas has been tested by several research groups, with DPF energies ranging from 100's of Joules to 100's of kJ. The results have varied significantly with some groups reporting enhancements under optimal conditions in excess of 30× and other groups reporting reduced yields compared to pure deuterium [23–28]. Our system was the first used to test such piston gases in a 100 J-class DPF. We utilized admixtures of deuterium and xenon with mass fractions ranging from 0% to 8%. However, over this range we failed to observe a statistically significant increase in neutron yield.

4. Discussion

A neutron producing nanofocus DPF has been constructed and characterized using a broad suite of synchronized diagnostics including a B-dot probe, fast neutron detectors, a high-speed framing camera, and laser imaging. It is this last point which makes this experimental setup unique, as we may obtain detailed information on the density evolution of the DPF plasma sheath on unprecedented short time and length scales. This resolution may be necessary to unfold the microscopic basis of neutron production in small DPFs, which necessitates observation of instabilities within the 100 micron-scale pinch in well-sub-ns times.

In measured performance, this device conforms to expectations regarding sheath velocity and (small DPF) neutron yield scaling. We have obtained insight into the electrical, radiative, and visual

characteristics of a DPF pulse on a shot-by-shot basis. A statistical approach to the calculation of neutron yield is described and employed, giving support to previous scaling laws.

While the performance of this DPF is at or slightly beyond the present frontier, it does not represent a significant extension of the state of the art, its complex of diagnostics does. In addition to framing camera with very short time capabilities, we have demonstrated the introduction of imaging using a 50 fs pulsed laser to produce shadowgraphs. The use of a coherent light source in this case may permit phase contrast imaging, which in turn opens the possibility of resolving separate sheath layers produced when one dopes a nominally deuterium-fed DPF with a heavy noble gas such as xenon. As this scheme is known to produce enhanced neutron production, it is a promising scenario for fundamental physics investigations that may give insight into the plasma dynamics involved.

Future work on development of the ultra-fast laser imaging system will include an extension of the laser image acquisition to a stroboscopic system (Figure 9). This system will be based on the existing 50 fs Ti:Sapphire laser combined with independent beam splitters, delay lines, and cameras. After running in pseudo-tomography mode to ensure a symmetrical discharge, the delay lines will be adjusted to stroboscopic mode, facilitating further exploration of the run-in and pinch dynamics based on single-shot analysis. This will reproduce the highly useful framing camera approach with much finer time resolution.

Finally, we note that the uniqueness of this instrument setup found in the diagnostic suite used may be used to investigate other classes of DPF. Most promising among these is a device based on a current transformer [22], which gives yet higher neutron yield at a given voltage used, due to enhancement of the current. This provides a stronger acceleration of the plasma sheath during run-in; a fundamental understanding of numerous physical aspects of this scenario would benefit from more precise diagnostic systems.

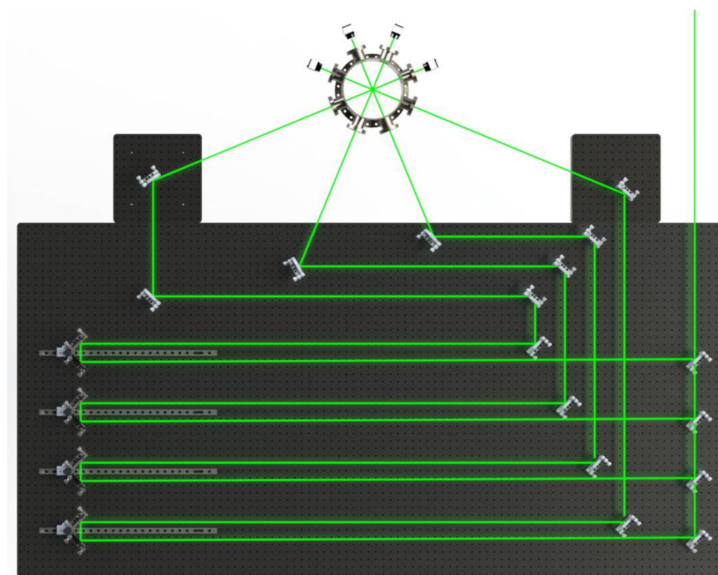


Figure 9. CAD model of a proposed stroboscopic imaging system showing four independent delay lines and cameras.

5. Patents

Two US provisional patents were produced from this work:

- 62/483,353—“Ultrafast, low jitter, spark gap”,
- 62/503,106—“Vacuum pumping aperture”.

Acknowledgments: This work was funded by the Defense Advanced Research Projects Agency (DARPA) program for Intense and Compact Neutron Sources (ICONS), award number HR0011-15-2-0013.

Conflicts of Interest: The authors declare no conflict of interest.

References

1. Moreno, C.; Bruzzone, H.; Martínez, J.; Clause, A. Conceptual Engineering of Plasma-Focus Thermonuclear Pulsors. *IEEE Trans. Plasma Sci.* **2000**, *28*, 1735–1741. [[CrossRef](#)]
2. Lee, S.; Kudryashov, V.; Lee, P.; Zhang, G.; Serban, A.; Liu, M.; Feng, X.; Springham, S.; Wong, T.; Selvam, C. Sxr Lithography Using a High Performance Plasma Focus Source. In Proceedings of the ICPP & 25th EPS Conference on Controlled Fusion and Plasma Physics, Praha, Czech Republic, 29 June–3 July 1998; Volume 22, pp. 2591–2594.
3. Hussein, E.M.A.; Waller, E.J. Review of one-side approaches to radiographic imaging for detection of explosives and narcotics. *Radiat. Meas.* **1998**, *29*, 581–591. [[CrossRef](#)]
4. Gibbons, M.R.; Richards, W.J.; Shields, K. Optimization of neutron tomography for rapid hydrogen concentration inspection of metal castings. *Nucl. Instrum. Methods Phys. Res. A* **1999**, *424*, 53–57. [[CrossRef](#)]
5. PhoenixLLC. Phoenix Neutron Generators. Available online: <https://www.phoenixwi.com/product/high-yield-neutron-generator/> (accessed on 18 October 2017).
6. Mather, J.W. Formation of a High-Density Deuterium Plasma Focus. *Phys. Fluids* **1965**, *8*, 366–377. [[CrossRef](#)]
7. Soto, L.; Pavez, C.; Moreno, J.; Barbaglia, M.; Clause, A. Nanofocus: An ultra-miniature dense pinch plasma focus device with submillimetric anode operating at 0.1 J. *Plasma Sources Sci. Technol.* **2008**, *18*, 15007. [[CrossRef](#)]
8. Gribkov, V.; Banaszak, A.; Bienkowska, B.; Dubrowsky, A.; Ivona-Stanik, I.; Jakubowski, L.; Karpinski, L.; Miklanzewski, R.; Paduch, M.; Sadowski, M.; et al. Plasma dynamics in the PF-1000 device under full-scale energy storage: II. Fast electron and ion characteristics versus neutron emission parameters and gun optimization perspectives. *J. Phys. D* **2007**, *40*, 3592. [[CrossRef](#)]
9. Lee, S.; Saw, S.H. Neutron Scaling Laws from Numerical Experiments. *J. Fusion Energy* **2008**, *27*, 292–295. [[CrossRef](#)]
10. Herold, H.; Kaeppler, H.J.; Schmidt, H.; Shakhatre, M.; Wong, C.S. Progress in Plasma Focus Operation up to 500 KJ Bank Energy. In Proceedings of the 12th Conference on Plasma Physics and Controlled Nuclear Fusion Research, Nice, France, 12–19 October 1988; Volume 2, p. 587.
11. Herold, H.; Jerzykiewicz, A.; Sadowski, M.; Schmidt, H. Comparative Analysis of Large Plasma Focus Experiments Performed at Ipf, Stuttgart, and at Ipj, Swierk. *Nucl. Fusion* **1989**, *29*, 1255. [[CrossRef](#)]
12. Moreno, J.; Silva, P.; Soto, L. Optical observations of the plasma motion in a fast plasma focus operating at 50 J. *Plasma Sources Sci. Technol.* **2002**, *12*, 39–45. [[CrossRef](#)]
13. Silva, P.; Soto, L.; Kies, W.; Moreno, J. Pinch evidence in a fast and small plasma focus of only tens of joules. *Plasma Sources Sci. Technol.* **2004**, *13*, 329. [[CrossRef](#)]
14. Soto, L.; Esaulov, A.; Moreno, J.; Silva, P.; Sylvester, G.; Zambra, M.; Nazarenko, A.; Clause, A. Transient electrical discharges in small devices. *Phys. Plasmas* **2001**, *8*, 2572–2578. [[CrossRef](#)]
15. Milanese, M.; Moroso, R.; Pouzo, J. D-D neutron yield in the 125 J dense plasma focus Nanofocus. *Eur. Phys. J. D* **2003**, *27*, 77–81. [[CrossRef](#)]
16. Silva, P.; Soto, L.; Moreno, J.; Sylvester, G.; Zambra, M.; Altamirano, L.; Clause, A.; Moreno, C.; Sylvester, G.; Zambra, M.; et al. A plasma focus driven by a capacitor bank of tens of joules. *Rev. Sci. Instrum.* **2002**, *73*, 2583–2587. [[CrossRef](#)]
17. Rout, R.K.; Mishra, P.; Rawool, A.M.; Kulkarni, L.V.; Gupta, S.C. Battery powered tabletop pulsed neutron source based on a sealed miniature plasma focus device. *J. Phys. D* **2008**, *41*, 205211. [[CrossRef](#)]
18. Verma, R.; Roshan, M.V.; Malik, F.; Lee, P.; Lee, S.; Springham, S.V.; Tan, T.L.; Krishnan, M.; Rawat, R.S. Compact sub-kilojoule range fast miniature plasma focus as portable neutron source. *Plasma Sources Sci. Technol.* **2008**, *17*, 45020. [[CrossRef](#)]
19. Soto, L.; Silva, P.; Moreno, J.; Zambra, M.; Kies, W.; Mayer, R.E.; Clause, A.; Altamirano, L.; Pavez, C.; Huerta, L. Demonstration of neutron production in a table-top pinch plasma focus device operating at only tens of joules. *J. Phys. D* **2008**, *41*, 205215. [[CrossRef](#)]

20. Bures, B.L.; Krishnan, M.; James, C. A Plasma Focus Electronic Neutron Generator. *IEEE Trans. Plasma Sci.* **2012**, *40*, 1082–1088. [[CrossRef](#)]
21. Shukla, R.; Sharma, S.K.; Banerjee, P.; Das, R.; Deb, P.; Prabakar, T.; Das, B.K.; Adhikary, B.; Shyam, A. Low voltage operation of plasma focus. *Rev. Sci. Instrum.* **2010**, *81*, 83501. [[CrossRef](#)] [[PubMed](#)]
22. Bures, B.L.; James, C.; Krishnan, M.; Adler, R. Application of an impedance matching transformer to a plasma focus. *Rev. Sci. Instrum.* **2011**, *82*, 78–83. [[CrossRef](#)] [[PubMed](#)]
23. Yap, S.L.; Wong, C.S.; Choi, P.; Dumitrescu, C.; Moo, S.P. Observation of two phases of neutron emission in a low energy plasma focus. *Jpn. J. Appl. Phys.* **2005**, *44*, 8125–8132. [[CrossRef](#)]
24. Verma, R.; Lee, P.; Springham, S.V.; Tan, T.L.; Rawat, R.S.; Krishnan, M. Order of magnitude enhancement in X-ray yield at low pressure deuterium-krypton admixture operation in miniature plasma focus device. *Appl. Phys. Lett.* **2008**, *92*, 11506. [[CrossRef](#)]
25. Mohammadi, M.A.; Sobhanian, S.; Rawat, R.S. Neutron production with mixture of deuterium and krypton in Sahand Filippov type plasma focus facility. *Phys. Lett. Sect. A Gen. At. Solid State Phys.* **2011**, *375*, 3002–3006. [[CrossRef](#)]
26. Talebitaher, A.; Lee, S.; Kalaiselvi, S.M.P.; Verma, R.; Lee, P.; Springham, S.V.; Tan, T.L.; Rawat, R.S. Influence of Krypton Doping on DD Fusion Neutron Production: An Evaluation Methodology for Optimization Level of Plasma Focus Device. *J. Fusion Energy* **2016**, *35*, 370–377. [[CrossRef](#)]
27. Aliaga-Rossel, R.; Choi, P. Experimental observations of the spatial anisotropy of the neutron emission in a medium energy plasma focus. *IEEE Trans. Plasma Sci.* **1998**, *26*, 1138–1145. [[CrossRef](#)]
28. Bures, B.L.; Krishnan, M.; Eshaq, Y. Controlling the neutron yield from a small dense plasma focus using deuterium-inert gas mixtures. *AIP Conf. Proc.* **2009**, *1088*, 195–198.
29. Clause, A.; Soto, L.; Tarifeno-Saldivia, A. Influence of the anode length on the neutron emission of a 50 J plasma focus: Modeling and experiment. *IEEE Trans. Plasma Sci.* **2015**, *43*, 629–636. [[CrossRef](#)]
30. Naranjo, B.; Gimzewski, J.K.; Putterman, S. Observation of nuclear fusion driven by a pyroelectric crystal. *Nature* **2005**, *434*, 1115–1117. [[CrossRef](#)] [[PubMed](#)]
31. Panigrahi, P.K.; Muralidhar, K. *Schlieren and Shadowgraph Methods in Heat and Mass Transfer*; Springer: New York, NY, USA, 2012; Volume 2, p. 139.
32. Haas, C.R.; Noll, R.; Ruhl, F.; Herziger, G. Schlieren Diagnostics of the Plasma Focus. *Nucl. Fusion* **1984**, *24*, 1216. [[CrossRef](#)]
33. Decker, G.; Deutsch, R.; Kies, W.; Rybach, J. Plasma Layers of Fast Focus Discharges—Schlierenpictures Experimentally Taken. *Plasma Phys. Control Fusion* **1985**, *27*, 609. [[CrossRef](#)]
34. Lee, S.; Serban, A. Dimensions and lifetime of the plasma focus pinch. *IEEE Trans. Plasma Sci.* **1996**, *24*, 1101–1105.
35. Tarifeno-Saldivia, A.; Mayer, R.; Pavez, C.; Soto, L. Methodology for the use of proportional counters in pulsed fast neutron yield measurements. *ArXiv* **2011**.
36. Soto, L.; Pavéz, C.; Moreno, J.; Altamirano, L.; Huerta, L.; Barbaglia, M.; Clause, A.; Mayer, R.E. Evidence of nuclear fusion neutrons in an extremely small plasma focus device operating at 0.1 Joules. *Phys. Plasmas* **2017**, *24*, 82703. [[CrossRef](#)]
37. Agostinelli, S. GEANT4—A simulation toolkit. *Nucl. Instrum. Methods Phys. Res. Sect. A* **2003**, *506*, 250–303. [[CrossRef](#)]
38. Soto, L. New trends and future perspectives on plasma focus research. *Plasma Phys. Control. Nucl. Fusion* **2005**, *47*, A361–A381. [[CrossRef](#)]
39. Tarifeno-Saldivia, A. *Estudio Experimental de una Descarga Plasma Focus Rapida Operada en el Rango de Decenas de Joules Emittiendo Neutrones*; Universidad de Concepción: Concepción, Chile, 2011.

